ARTICLE

doi:10.1038/nature11400

Antibiotics in early life alter the murine colonic microbiome and adiposity

Ilseung Cho[1,2], Shingo Yamanishi[1], Laura Cox[3], Barbara A. Methé[4], Jiri Zavadil[5,6], Kelvin Li[4], Zhan Gao[3], Douglas Mahana[3], Kartik Raju[3], Isabel Teitler[3], Huilin Li[7], Alexander V. Alekseyenko[1,6] & Martin J. Blaser[1,2,3]

Antibiotics administered in low doses have been widely used as growth promoters in the agricultural industry since the 1950s, yet the mechanisms for this effect are unclear. Because antimicrobial agents of different classes and varying activity are effective across several vertebrate species, we proposed that such subtherapeutic administration alters the population structure of the gut microbiome as well as its metabolic capabilities. We generated a model of adiposity by giving subtherapeutic antibiotic therapy to young mice and evaluated changes in the composition and capabilities of the gut microbiome. Administration of subtherapeutic antibiotic therapy increased adiposity in young mice and increased hormone levels related to metabolism. We observed substantial taxonomic changes in the microbiome, changes in copies of key genes involved in the metabolism of carbohydrates to short-chain fatty acids, increases in colonic short-chain fatty acid levels, and alterations in the regulation of hepatic metabolism of lipids and cholesterol. In this model, we demonstrate the alteration of early-life murine metabolic homeostasis through antibiotic manipulation.

Antibiotics, discovered in the early twentieth century, came into widespread use after the Second World War, with substantial public health benefits. Antibiotic use has increased markedly, now approximating one antibiotic course per year in the average child in the United States[1,2]. However, there is increasing concern that antibiotic exposure may have long-term consequences[3–5].

For more than 50 years we have known that the administration of low doses of antibacterial agents promotes the growth of farm animals, consequently, in the United States, the largest use of antibiotics and related antimicrobial substances is within farms, with low doses fed to large numbers of animals used for food production to increase weight gain by as much as 15%[6,7]. These effects are broad across vertebrate species, including mammals (cattle, swine, sheep) and birds (chickens, turkeys), and follow oral administration of the agents, either in feed or water, indicating that the microbiota of the gastrointestinal (GI) tract is a major target. That the effects are observed with many different classes of antibacterial agents (including macrolides, tetracyclines, penicillins and ionophores) indicates that the activity is not an agent-specific side effect, nor have the effects been observed with antifungals or antivirals.

The vertebrate GI tract contains an exceptionally complex and dense microbial environment, with bacterial constituents that affect the immune responses of populations of reactive host cells[8] and stimulate a rich matrix of effecter mechanisms involved in innate and adaptive immune responses[9]. The GI tract also is a locus of hormone production, including those involved in energy homeostasis (such as insulin, glucagon, leptin and ghrelin) and growth (for example, glucose-dependent insulinotropic polypeptide (GIP) and glucagon-like peptide 1 (GLP-1))[10]. Alterations in the populations of the GI microbiota may change the intra-community metabolic interactions[11], modify caloric intake by using carbohydrates such as cellulose that are otherwise indigestible by the host[12], and globally affect host metabolic, hormonal and immune homeostasis[13]. Full (therapeutic) dose antibiotic treatments alter both the composition of the gastrointestinal microbiota[14] and host responses to specific microbial signals[15]. In combination with dietary changes, antibiotic administration has been associated with changes in the population structure of the microbiome. However, the effects of exposure to subtherapeutic antibiotic dosages have not been described.

Early studies of the effects of gut microbiota on metabolism were limited by the use of culture-based technologies that interrogated $<5\%$ of the extant GI tract microbes[16]. Culture-independent investigation of small-subunit ribosomal RNA sequences allows the microbial population structure[17] of the gut microbiota to be characterized with greater resolution. Despite inter-individual differences, substantial similarities exist[18] among mammalian species in the GI microbiota at higher taxonomic levels and functional pathways, indicating a basis for the conserved responses to early-life subtherapeutic antibiotic treatment (STAT) within farms. Previous work has shown that obesity leads to variation in the GI microbiome[12,19]; we use the insights provided from modern agricultural practices to suggest an alternative approach, using a murine model of STAT to explore how antibiotic exposure modulates host metabolic phenotypes.

Early-life STAT increases adiposity

We exposed C57BL/6J mice at weaning to penicillin, vancomycin, penicillin plus vancomycin, chlortetracycline, or no antibiotic in their drinking water at levels in the mid-range of US Food and Drug Administration (FDA)-approved levels for subtherapeutic antibiotic use in agriculture[6,7]. After a 7 week exposure, the observed weights were within the expected range of growth for female C57BL/6J mice, and there was no significant difference in overall growth between the STAT and control mice (Fig. 1a). However, by dual energy X-ray absorptiometry (DEXA) scanning, (Fig. 1b) total fat mass was significantly higher in all four groups of STAT mice than in the control group (Fig. 1c). Per cent body fat also was increased in most STAT groups compared to controls (Fig. 1d). Lean weight was not significantly ($P = 0.24$) different in the STAT mice (15.0 ± 0.1 g (mean $\pm$ standard error)) compared to controls (15.4 ± 0.3 g)

[1]Department of Medicine, New York University School of Medicine, New York, New York 10016, USA. [2]Medical Service, VA New York Harbor Healthcare System, New York, New York 10010, USA. [3]Department of Microbiology, New York University School of Medicine, New York, New York 10016, USA. [4]J. Craig Venter Institute, Rockville, Maryland 20850, USA. [5]Department of Pathology, New York University School of Medicine, New York, New York 10016, USA. [6]Center for Health Informatics and Bioinformatics, New York University School of Medicine, New York, New York 10016, USA. [7]Department of Population Health, New York University School of Medicine, New York, New York 10016, USA.

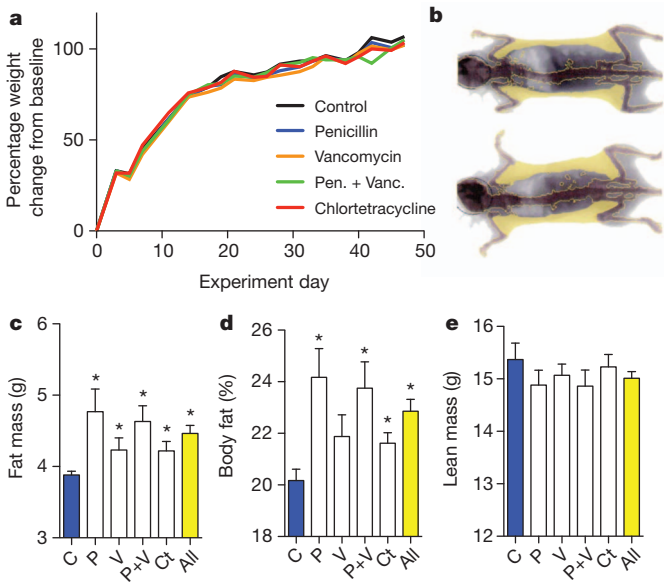

Figure 1 | Weight and body composition of control and STAT mice. **a**, Weight gain did not differ between control and STAT mice ($n = 10$ mice per group). **b**, Representative DEXA show per cent body fat in control (22.9%; top) and STAT (32.0%; bottom) mice. **c**, Total fat mass was significantly increased ($^*P < 0.05$) in all STAT groups compared to controls. **d**, Per cent body fat was significantly increased in all STAT groups (all $P < 0.05$) except vancomycin. **e**, Lean mass was lower in STAT mice, but not significantly different from controls. Data are presented as mean ± s.e.m. For all figures: all, all antibiotics; C, controls; Ct, chlortetracycline; P, penicillin; P+V, penicillin plus vancomycin; V, vancomycin.

(Fig. 1e). Thus, 7 weeks after starting the intervention, each of several STAT exposures changed body composition but not overall weight. Repeat STAT experiments showed similar results (Supplementary Fig. 2). There were no significant differences in calculated feed efficiency, expressed as weight gained per unit of feed consumed, between the STAT and control mice. In a larger, confirmatory experiment to assess when the morphometric changes appear, we began examining the mice immediately at weaning. Both the STAT males and females showed significantly increased early life growth rates (Supplementary Fig. 3A), and fat mass in the STAT animals began to diverge from controls by 16–20 weeks, in both males and females. Between 8 and 26 weeks, there were significantly increased rates of fat accumulation in both female and male STAT mice (0.042 and 0.045 g week^{-1}, respectively) compared to controls; female mice also showed significantly increased total mass (Supplementary Fig. 3B). These studies confirm the increased adiposity associated with STAT in females, show parallel effects in males, and indicate that the morphometric changes begin at the earliest time (day 22) of measurement.

Bone mineral density is increased in early-life growth

Bone mineral density (BMD) was evaluated by DEXA scanning in the control and STAT mice after 3 and 7 weeks of exposure. At 3 weeks, the BMDs in each of the five STAT groups (and overall) was significantly increased compared to controls (Fig. 2a). By 7 weeks, the BMDs in all mice increased, without significant differences between the STAT (0.045 ± 0.002 mg cm^{-2}) and control mice (0.046 ± 0.003 mg cm^{-2}) (Fig. 2a). Thus, an early bone developmental phenotype observed in each of the STAT groups normalized by 7 weeks. Parallel observations have been made in other STAT experiments (data not shown).

Increased GIP in STAT mice

To examine metabolic correlates to the changes in body composition, we assessed GIP, an incretin synthesized by small intestinal K cells[20] with receptors located on adipocytes that stimulates lipoprotein

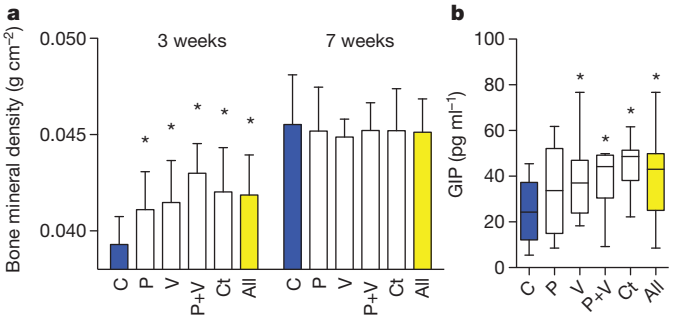

Figure 2 | Bone development and serum GIP measurements. **a**, After 3 weeks of STAT, bone mineral density was significantly increased in each group ($n = 10$ mice per group) compared to controls ($^*P < 0.05$) but did not persist at 7 weeks. **b**, Serum GIP levels measured at death were significantly increased in the vancomycin, penicillin plus vancomycin, and chlortetracycline groups and in the aggregate antibiotic group compared to controls ($P < 0.05$). Data are presented as mean ± s.e.m. Box plots show median ± interquartile range (IQR) and 95% ranges (whiskers).

lipase activity[21]. GIP was significantly elevated in the STAT mice (39.1 ± 2.5 pg ml^{-1}) compared to controls (24.4 ± 4.2 pg ml^{-1}), with the levels ranging from 34.3 ± 6.1 pg ml^{-1} in the penicillin group to 44.9 ± 3.7 pg ml^{-1} in the chlortetracycline group (Fig. 2b). Increases in GIP levels are consistent with existing mouse models of obesity, such as in IRS-1/GIPR and Kir6.2/GIPR double knockout mice that show increased levels of GIP, adiposity and serum glucose[22,23]. GIP elevation in STAT mice provides a mechanism for the observed adiposity increase[24,25], but also could be secondary to the metabolic changes. There were no significant differences for fasting insulin-like growth factor (IGF)-I, insulin, peptide YY, leptin, or ghrelin levels between control and STAT mice (Supplementary Fig. 4). Glucose tolerance tests performed during week 6 of the experiment showed a trend towards hyperglycaemia in STAT mice (Supplementary Fig. 5).

STAT does not alter overall gut microbial census

To determine whether the STAT exposure leading to these metabolic changes affected the GI tract microbiome, microbial DNA extracted from faecal and caecal samples collected from the mice during the week of euthanasia or at necropsy, respectively, were studied. DNA concentrations measured from both caecal (77.62 ± 33.51 ng µl^{-1}) and faecal (23.79 ± 14.41 ng µl^{-1}) samples were not significantly different between control ($n = 10$) and STAT mice ($n = 10$ per group). The census in the STAT and control mice, determined through quantitative PCR using 338F/518R universal primers (Supplementary Table 1), showed no significant differences in bacterial counts or fungal census among the STAT and control groups (Fig. 3a). These data indicated that STAT exposure did not lead to substantial changes in the overall microbial census, and next led to us to conduct an assessment of the composition of the populations.

STAT alters the composition of intestinal microbiota

To assess microbial populations in the STAT and control microbiomes, we analysed the relative distribution of taxonomic groups based on 16S rRNA v3 region sequence data. The extracted DNA was subjected to 454 pyrosequencing, yielding 555,233 readable sequences (5,784 ± 676 sequences per sample with mean length 188 ± 3 bp). The sequences were analysed at multiple (phylum to genus) taxonomic levels (Supplementary Fig. 6 and Supplementary Table 2). In both faecal and caecal samples, the ratio of Firmicutes to Bacteria was significantly elevated in the STAT mice compared to controls (Fig. 3b and Supplementary Fig. 7). Weighted Unifrac analysis of the dominant taxa (present in >1% of the total population) showed a nonrandom clustering of STAT and control mice ($P < 0.05$) (Fig. 3c). Importantly, deep branching was identified, with the mean weight of mice on the two major branch points on the heat map being

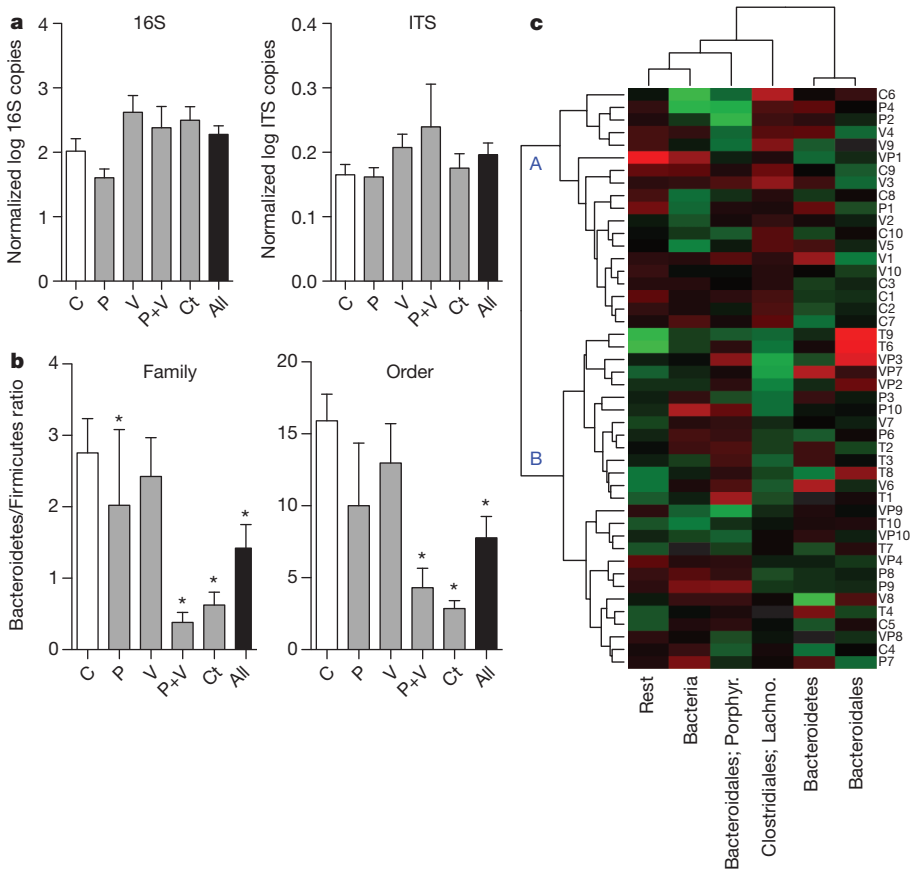

Figure 3 | Changes in the faecal gut microbiome after 50 days of STAT. **a**, There were no significant differences in microbial census between the STAT and control groups ($n = 10$ mice per group) evaluated by qPCR with universal primers for 16S rRNA and internal transcribed spacer (ITS). **b**, By 454-pyrosequencing, Firmicutes were shown to be increased in the STAT mice at multiple taxonomic levels. (Controls $n = 10$, penicillin $n = 9$, vancomycin $n = 10$, penicillin plus vancomycin $n = 8$, chlortetracycline $n = 10$; $^*P < 0.05$.) Data are presented as mean ± s.e.m. **c**, Heat map of specimens showing relative abundance of bacteria present at >1% at the family taxonomic level. Hierarchical clustering based on Euclidean distance identified nonrandom branch distributions of control and STAT mice ($P < 0.05$). Lachno., Lachnospiraceae; Porphyr., Porphyromonadaceae.

significantly ($P < 0.05$) different (21.4 ± 3.1% (point A) versus 23.0 ± 2.8% (point B); Fig. 3c). A major contributor to the observed differences is increased Lachnospiraceae representation in the STAT mice. Minor taxonomic groups may have roles in the development of metabolic phenotypes, and STAT-associated increases in several minor taxa are consistent with this possibility (Supplementary Table 3). Additional rarefaction curves and Unifrac analyses, quantile plots, PCoA representations, and heat maps generated using non-Euclidean distance metrics (Supplementary Figs 8–11 and http://www.med.nyu.edu/medicine/labs/blaserlab/PDFs/Cho-et-al-Online-Figures.pdf) demonstrated consistent shifts within the microbial populations in the STAT-exposed groups. Although STAT did not change the overall bacterial census, even the minimal antibiotic doses caused shifts in taxonomic composition, such as the Lachnospiraceae bloom. We noted an increase in the relative concentrations of Firmicutes compared to Bacteroidetes in the STAT mice compared to controls, which accompanied the observed increases in adiposity. This observation extends previous findings[26,27] of relative increases in the Firmicute population in *ob/ob* mice that are genetically prone to obesity. However, observations at such high taxonomic strata may not sufficiently describe the changes associated with obesity[28,29]; variations in DNA extraction efficiency and PCR-based sequencing of complex, heterogeneous microbial communities may bias census estimates of specific bacterial taxa. Furthermore, although the overall phenotypes (increased adiposity and hepatic lipogenesis) are consistent in the STAT groups, the intermediate steps may be more host- and treatment-specific. Our findings indicate that specific STAT exposures can be used as probes of microbiome structure and function.

STAT exposure alters gut microbiome SCFA metabolism

Because of the central role of short-chain fatty acid (SCFA) synthesis in colonic metabolism[30,31], we examined the effect of STAT exposure on the gene counts of prokaryotic genes butyryl coA transferase (BCoAT) and formyltetrahydrofolate synthetase (FTHFS) that are involved in butyrate and acetate synthesis, respectively (Supplementary Fig. 12). Quantitative PCRs (qPCRs) for total bacteria, and degenerate qPCRs for BCoAT and FTHFS, were performed on caecal specimens in control and STAT mice. At 3 weeks, there were significant decreases in BCoAT gene copy numbers in the penicillin plus vancomycin, chlortetracycline, and aggregate groups. By 6 weeks, BCoAT copy numbers had increased in all the groups compared to the 3-week values, but there was no longer an aggregate difference. For FTHFS overall, there were no significant differences between control and STAT mice overall at 3 or 6 weeks, although there was variation within the antibiotic groups (Fig. 4a). Exploring the inter-antibiotic differences further, we noted that there were several patterns in the FTHFS qPCR with different melting curve peaks (Supplementary Fig. 13), indicating differences in the microbial population. In total, these results provide evidence that STAT treatment is dynamically affecting composition of genes related to SCFAs, probably in antibiotic-specific ways, but with overall conserved effects. Both BCoAT and FTHFS have a role in metabolism of carbohydrates into SCFAs[32] and have been used to assess the functional characteristics of complex communities[33]; the observed changes in gene copy numbers in young STAT mice relative to controls as well as changes at different time points provide evidence that the STAT colonic microbiome alters SCFA metabolism. Our finding that the copy numbers of these

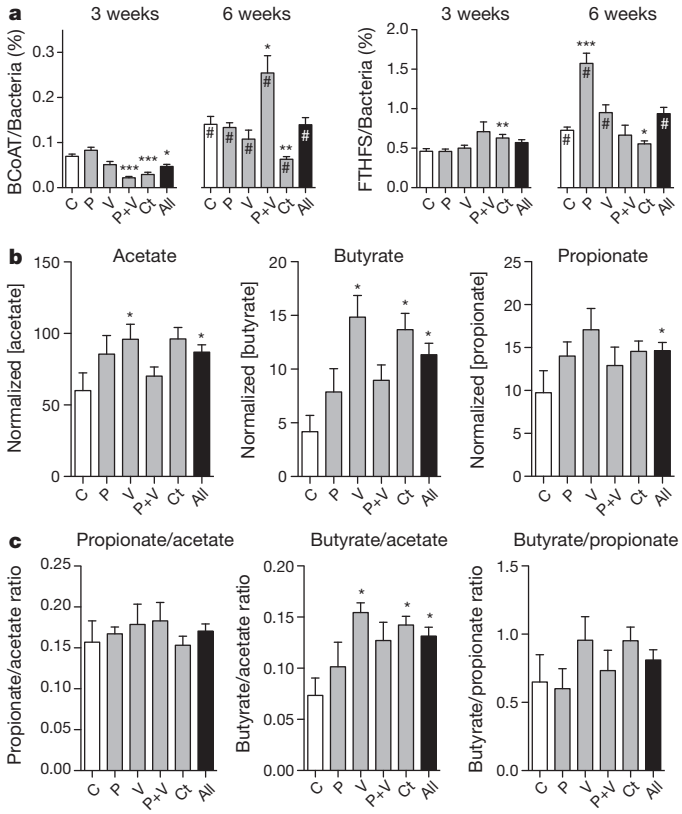

Figure 4 | Caecal SCFA production after STAT exposure. **a**, Quantitative PCR was performed for butyryl CoA transferase (BCoAT) and formyltetrahydrofolate synthetase (FTHFS) at experiment weeks 3 and 6 on STAT and control groups ($n = 10$ mice per group). At 3 weeks, BCoAT was diminished in two STAT groups and the aggregate group, a difference that persisted only in the chlortetracycline group. FTHFS copies do not show a consistent pattern. $^{*}P < 0.05$, $^{**}P < 0.01$, $^{***}P < 0.001$ comparing STAT to controls; hash symbol indicates significant difference between 3 and 6 weeks. **b**, SCFA concentration analysed by gas chromatography (GC) shows increases in SCFAs in each of the STAT groups compared to controls. **c**, The ratio of butyrate relative to acetate is significantly higher in the STAT mice than controls. Data are presented as mean ± s.e.m.

two genes increase during growth (between 3 and 6 weeks) in both control and STAT mice (Fig. 4) suggests a greater dependence on SCFA synthesis pathways with maturation. Relative differences in the extent of these changes and in the melting curve peak populations may reflect changes in microbial populations. Furthermore, gene copy number (Fig. 4) in conjunction with melting curve peak patterns (Supplementary Fig. 13) may be useful for studying community genotypes of metabolic potential.

Direct measurements of SCFAs in the caecal contents of control and STAT mice demonstrate substantial increases in acetate, propionate and butyrate in all STAT groups (Fig. 4b); ratios of butyrate to acetate are also significantly altered by STAT exposure (Fig. 4c). These findings provide evidence that STAT exposure perturbs not only the composition of the GI microbiome but also the metabolic capabilities of the microbiome, specifically with respect to SCFAs. Increased SCFA concentrations and butyrate/acetate levels provide mechanisms for the STAT-induced adiposity phenotypes. SCFAs directly provide energy to colonocytes, and absorption into the portal circulation stimulates adipogenesis[30,34]. Metabolic cage experiments examining metabolic balance show no significant difference in caloric intake between control and STAT mice but lower caloric output in faecal pellets from STAT mice (Supplementary Fig. 14), providing evidence for selection for microbiota that can extract calories from otherwise indigestible constituents.

STAT alters hepatic metabolism of fatty acids and lipids

In confirmatory experiments using the identical STAT penicillin protocol, liver tissue was collected from both control and STAT mice. Standard histological analysis and triglyceride measurements showed no significant differences between control and STAT mice (Supplementary Fig. 15a, b). There were no significant differences in 16S rRNA gene counts, as detected by qPCR, from the liver specimens, providing evidence that bacterial translocation is not altered in the STAT mice (Supplementary Fig. 15c). Microarray analyses surveyed for differences in >45,000 genes, identifying 466 that by *t*-test or post translational modification statistics (PTM) were significantly up- or downregulated (397 significantly differed from controls by both tests) in the STAT compared to control mice. Focusing on pathways related to fatty acid metabolism and lipid metabolic processes, 22 and 47 genes, respectively, were differentially expressed between STAT and control mice (Fig. 5a). When specific genes were mapped to murine hepatic metabolic pathways, there were consistent changes in the same direction for several pathways, including upregulation in pathways related to lipogenesis and triglyceride synthesis (Fig. 5b). The changes in gene expression observed by microarray analyses were extended by qPCR assays of the same genes (Supplementary Fig. 16). These microarray and qPCR findings demonstrate substantial changes in the regulation of hepatic lipid, cholesterol and triglyceride metabolism that result from STAT-induced intraluminal intestinal changes.

Increased STAT adiposity is not metabolically altered

In the same confirmatory experiments (Supplementary Fig. 3), visceral adipose tissue dissected from control and STAT (penicillin) mice had no significant differences in adipocyte counts (Supplementary Fig. 17a, c) or in immunohistochemical staining for $CD68^{+}$ macrophages (Supplementary Fig. 17b, d). These findings were extended by *Gapdh*-normalized (Supplementary Fig. 17e) metabolic gene qPCR analyses. There were no significant differences in leptin, adiponectin, resistin, sterol regulatory element binding transcription factor 1 (*Srebf1*, also called *SREBP1c*), peroxisome proliferator activated receptor γ (*Pparg*, also called *PPARγ2*), and fatty acid synthase (*Fasn*, also called *FAS*) levels between the control and STAT groups (Supplementary Fig. 17f). These findings provide evidence that STAT adipose tissue shows no substantial physiological difference compared to controls in cell density, local inflammation, or metabolic potential as demonstrated by quantitative PCR. Increased adiposity seems to be a downstream phenomenon primarily mediated by changes in the gut and liver.

Discussion

By developing a model to assess adiposity, we show that each of the several STAT approaches tested affects the adiposity of post-weaning C57BL/6J mice. Similarly, there was a consistent early change in bone development. Particularly in the dynamic phases of growth in young animals, STAT alterations of the microbiome may affect pluripotent cells that can become osteoblasts, adipocytes, or myocytes. Although the STAT model does not precisely replicate the weight gain observed in farm animals, possibly due to differences in the husbandry of laboratory mice in a clean environment versus animals raised on a farm, the broad effects of exposure demonstrated in this model provide evidence that altering the microbiome may have substantial consequences. Such changes in early-life body composition may be due to altered host responses[35,36] and/or shifts in the metabolic characteristics of the gut microbiome. We postulate that the STAT exposures selected for microbiota with increased metabolic activity that were able to extract a higher proportion of calories from dietary complex carbohydrates that were relatively indigestible in the control mice. The increased SCFA concentrations are the metabolic products of this activity, which then may be delivered in increased quantities through the portal circulation to the liver, enabling enhanced lipogenesis (Supplementary Fig. 18). Enhanced caloric absorption has been implicated as a mechanism for increased weight gain in other murine obesity models[12]. The observed increase in

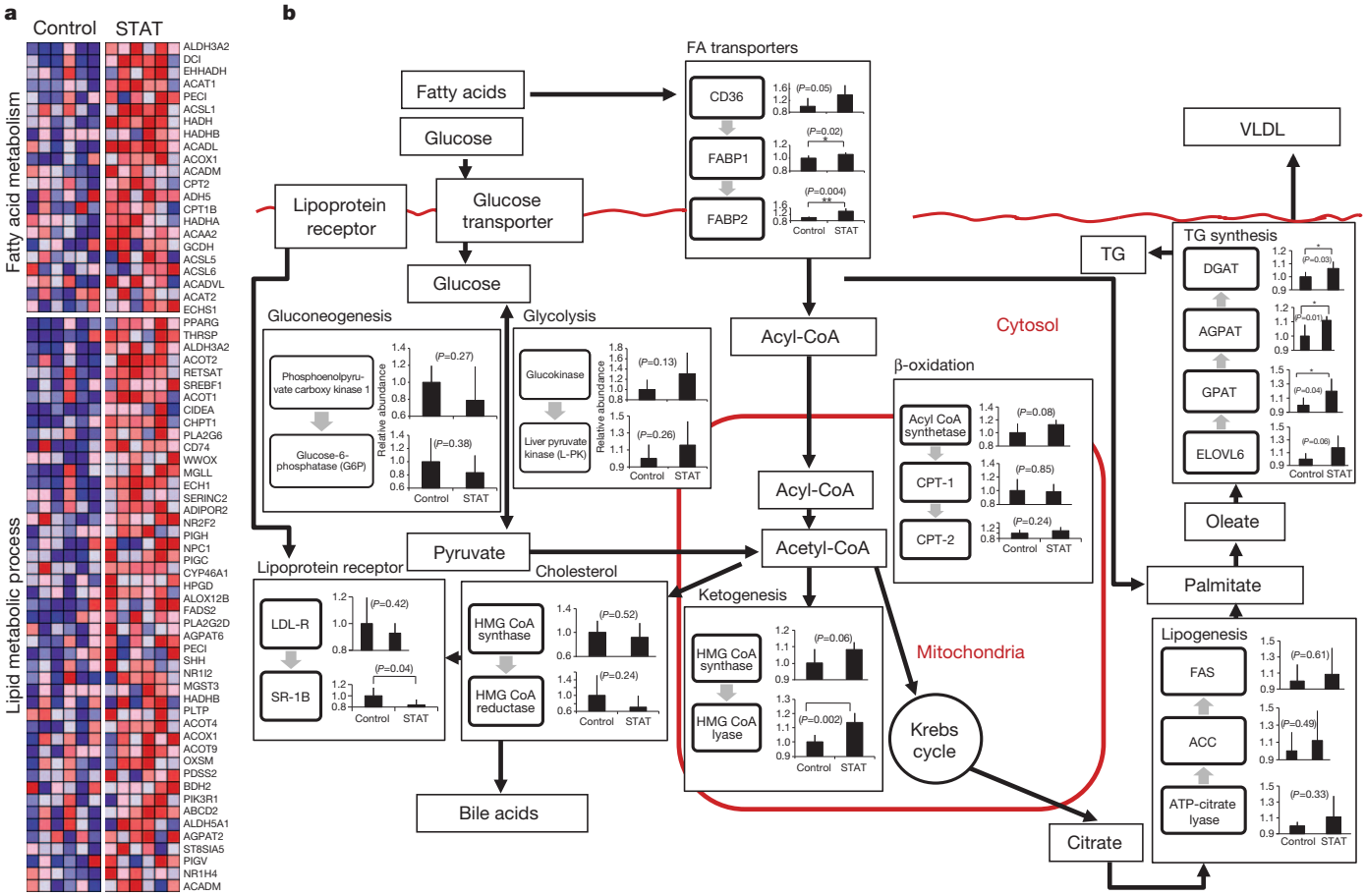

Figure 5 | Differentially regulated genes related to hepatic lipogenesis, identified through microarray and quantitative PCR analyses. a, Microarray analysis of liver specimens surveyed for differences in >45,000 genes; 397 genes were significantly up- or downregulated. Heat maps generated by gene set enrichment analysis (GSEA)[43] identify differences between the STAT and control mice ($n = 6$ mice per group), including pathways related to fatty acid metabolism and lipid metabolic processes. **b**, Mapping of metabolic genes detected by microarray onto specific pathways, including those related to lipogenesis and triglyceride synthesis, show consistent changes with STAT. Data are presented as mean ± s.e.m. White bars, controls; black bars, STAT; $*P < 0.05$, $**P < 0.01$. TG, triglycerides; VLDL, very low-density lipoproteins.

adiposity is similar across several different STAT exposures, despite the different antibiotics used. This is consistent with the observation that a wide range of FDA-approved antibacterial agents are used for effective growth promotion in the agricultural industry[6,7,37]. Our studies of the intestine, liver and adipose tissue demonstrate that the active effect of the antibiotics is on the microbiota affecting the downstream liver; mechanistically, the adipose tissue is passively accepting the increased lipid load produced from more proximal activities.

Why might STAT exposures have such substantial effects on recipient animals? We propose that STAT represents a compounded perturbation, as described previously[38], that has more serious consequences for long-term alterations of community state, possibly generating a different assemblage of species. The STAT-induced increase in SCFA production is a change in substrate availability that is a characteristic[39] of ecological disturbance. Such overharvesting, at a developmentally sensitive time, may push the ecosystem beyond the normative recovery that usually follows infrequent disturbances[38]. In complex, co-evolved ecosystems, the intricate interactions among participants conform to equilibria[40] that promote the robustness of a community[41]. However, when such equilibria are substantially perturbed, changes in host health and disease may result[42]. Other causative mechanisms for the changes in host phenotype could reflect that maturation of the gut microbiome is temporally altered by STAT exposure or that host responses are altered by microbiome changes. Ultimately, the interaction between the microbiome's metabolic capabilities and numerous host reactive cells could account for the observed changes, including the increase in GIP. In our study, we confirm in a tractable experimental model the decades-long observations in farm animals that STAT exposure changes host development, and we demonstrate specific techniques useful for studying the metabolic effects of microbiome manipulation. Our study also indicates the possibility that modulation of the infant human gut microbiome by antibiotics could have long-term metabolic consequences affecting adiposity and bone development.

METHODS SUMMARY

Female C57BL/6J mice were given penicillin, vancomycin, penicillin plus vancomycin, or chlortetracycline (1 μg antibiotic per g body weight) via drinking water, or no antibiotics (control). Body weight was serially measured and body composition determined using dual energy X-ray absorptiometry (DEXA). At death, blood, caecal contents, liver and visceral adipose tissue were collected, and serum hormones measured. DNA was extracted from caecal contents and faecal pellets, and 16S rRNA gene v3 regions were barcoded and sequenced, using 454-FLX Titanium chemistry. Quality-filtered sequences were processed through the QIIME pipeline and analysed in the R statistical environment. Quantitative PCR assessed taxa and metabolic genes of interest, and expression profiling of hepatic RNA was performed by microarray.

Full Methods and any associated references are available in the online version of the paper.

Received 1 April 2011; accepted 6 July 2012.
Published online 22 August 2012.

1. McCaig, L. F. & Hughes, J. M. Trends in antimicrobial drug prescribing among office-based physicians in the United States. *J. Am. Med. Assoc.* **273,** 214–219 (1995).

2. Kozyrskyj, A. L., Ernst, P. & Becker, A. B. Increased risk of childhood asthma from antibiotic use in early life. *Chest* **131,** 1753–1759 (2007).
3. Blaser, M. J. & Falkow, S. What are the consequences of the disappearing human microbiota? *Nature Rev. Microbiol.* **7,** 887–894 (2009).
4. Dethlefsen, L. & Relman, D. A. Microbes and Health Sackler Colloquium: Incomplete recovery and individualized responses of the human distal gut microbiota to repeated antibiotic perturbation. *Proc. Natl Acad. Sci. USA* **108,** 4554–4561 (2010).
5. Manichanh, C. *et al.* Reshaping the gut microbiome with bacterial transplantation and antibiotic intake. *Genome Res.* **20,** 1411–1419 (2010).
6. Butaye, P., Devriese, L. A. & Haesebrouck, F. Antimicrobial growth promoters used in animal feed: effects of less well known antibiotics on gram-positive bacteria. *Clin. Microbiol. Rev.* **16,** 175–188 (2003).
7. Ozawa, E. Studies on growth promotion by antibiotics. *J. Antibiot.* **8,** 205–214 (1955).
8. Abreu, M. T., Fukata, M. & Arditi, M. TLR signaling in the gut in health and disease. *J. Immunol.* **174,** 4453–4460 (2005).
9. Qin, J. *et al.* A human gut microbial gene catalogue established by metagenomic sequencing. *Nature* **464,** 59–65 (2010).
10. Hansotia, T. & Drucker, D. J. GIP and GLP-1 as incretin hormones: lessons from single and double incretin receptor knockout mice. *Regul. Pept.* **128,** 125–134 (2005).
11. Gesta, S., Tseng, Y. H. & Kahn, C. R. Developmental origin of fat: tracking obesity to its source. *Cell* **131,** 242–256 (2007).
12. Turnbaugh, P. J. *et al.* An obesity-associated gut microbiome with increased capacity for energy harvest. *Nature* **444,** 1027–1031 (2006).
13. Reikvam, D. H. *et al.* Depletion of murine intestinal microbiota: effects on gut mucosa and epithelial gene expression. *PLoS ONE* **6,** e17996 (2011).
14. Robinson, C. J. & Young, V. B. Antibiotic administration alters the community structure of the gastrointestinal micobiota. *Gut Microbes* **1,** 279–284 (2010).
15. Wlodarska, M. *et al.* Antibiotic treatment alters the colonic mucus layer and predisposes the host to exacerbated *Citrobacter rodentium*-induced colitis. *Infect. Immun.* **79,** 1536–1545 (2011).
16. McCracken, V. J., Simpson, J. M., Mackie, R. I. & Gaskins, H. R. Molecular ecological analysis of dietary and antibiotic-induced alterations of the mouse intestinal microbiota. *J. Nutr.* **131,** 1862–1870 (2001).
17. Pace, N. R. A molecular view of microbial diversity and the biosphere. *Science* **276,** 734–740 (1997).
18. Spor, A., Koren, O. & Ley, R. Unravelling the effects of the environment and host genotype on the gut microbiome. *Nature Rev. Microbiol.* **9,** 279–290 (2011).
19. Ley, R. E. *et al.* Obesity alters gut microbial ecology. *Proc. Natl Acad. Sci. USA* **102,** 11070–11075 (2005).
20. Buffa, R. *et al.* Identification of the intestinal cell storing gastric inhibitory peptide. *Histochemistry* **43,** 249–255 (1975).
21. Miyawaki, K. *et al.* Inhibition of gastric inhibitory polypeptide signaling prevents obesity. *Nature Med.* **8,** 738–742 (2002).
22. Tsukiyama, K. *et al.* Gastric inhibitory polypeptide is the major insulinotropic factor in K_{ATP} null mice. *Eur. J. Endocrinol.* **151,** 407–412 (2004).
23. Zhou, H. *et al.* Gastric inhibitory polypeptide modulates adiposity and fat oxidation under diminished insulin action. *Biochem. Biophys. Res. Commun.* **335,** 937–942 (2005).
24. Yip, R. G., Boylan, M. O., Kieffer, T. J. & Wolfe, M. M. Functional GIP receptors are present on adipocytes. *Endocrinology* **139,** 4004–4007 (1998).
25. Yamada, Y. & Seino, Y. Physiology of GIP—a lesson from GIP receptor knockout mice. *Horm. Metab. Res.* **36,** 771–774 (2004).
26. Ley, R. E. *et al.* Obesity alters gut microbial ecology. *Proc. Natl Acad. Sci. USA* **102,** 11070–11075 (2005).
27. Turnbaugh, P. J., Backhed, F., Fulton, L. & Gordon, J. I. Diet-induced obesity is linked to marked but reversible alterations in the mouse distal gut microbiome. *Cell Host Microbe* **3,** 213–223 (2008).
28. Murphy, E. F. *et al.* Composition and energy harvesting capacity of the gut microbiota: relationship to diet, obesity and time in mouse models. *Gut* **59,** 1635–1642 (2010).
29. Fleissner, C. K. *et al.* Absence of intestinal microbiota does not protect mice from diet-induced obesity. *Br. J. Nutr.* **104,** 919–929 (2010).
30. Wong, J. M., de Souza, R., Kendall, C. W., Emam, A. & Jenkins, D. J. Colonic health: fermentation and short chain fatty acids. *J. Clin. Gastroenterol.* **40,** 235–243 (2006).
31. Hong, Y. H. *et al.* Acetate and propionate short chain fatty acids stimulate adipogenesis via GPCR43. *Endocrinology* **146,** 5092–5099 (2005).
32. Lovell, C. R. & Leaphart, A. B. Community-level analysis: key genes of CO_2-reductive acetogenesis. *Methods Enzymol.* **397,** 454–469 (2005).
33. Henderson, G., Naylor, G. E., Leahy, S. C. & Janssen, P. H. Presence of novel, potentially homoacetogenic bacteria in the rumen as determined by analysis of formyltetrahydrofolate synthetase sequences from ruminants. *Appl. Environ. Microbiol.* **76,** 2058–2066 (2010).
34. Bergman, E. N. Energy contributions of volatile fatty acids from the gastrointestinal tract in various species. *Physiol. Rev.* **70,** 567–590 (1990).
35. Backhed, F. *et al.* The gut microbiota as an environmental factor that regulates fat storage. *Proc. Natl Acad. Sci. USA* **101,** 15718–15723 (2004).
36. Backhed, F., Ley, R. E., Sonnenburg, J. L., Peterson, D. A. & Gordon, J. I. Host-bacterial mutualism in the human intestine. *Science* **307,** 1915–1920 (2005).
37. Jukes, T. H. Antibiotics in animal feeds. *N. Engl. J. Med.* **282,** 49–50 (1970).
38. Paine, R. T., Tegner, M. J. & Johnson, E. A. Compounded perturbations yield ecological surprises. *Ecosystems* **1,** 535–545 (1998).
39. Pickett, S. T. & White, P. S. *The Ecology of Natural Disturbance and Patch Dynamics* (Academic, 1985).
40. Blaser, M. J. & Kirschner, D. The equilibria that allow bacterial persistence in human hosts. *Nature* **449,** 843–849 (2007).
41. Sole, R. V. & Montoya, J. M. Complexity and fragility in ecological networks. *Proc. R. Soc. Lond. B* **268,** 2039–2045 (2001).
42. Cho, I. & Blaser, M. J. The human microbiome: at the interface of health and disease. *Nature Rev. Genet.* **13,** 260–270 (2012).
43. Subramanian, A. *et al.* Gene set enrichment analysis: a knowledge-based approach for interpreting genome-wide expression profiles. *Proc. Natl Acad. Sci. USA* **102,** 15545–15550 (2005).

Supplementary Information is available in the online version of the paper.

Acknowledgements This work was supported in part with grants from the NIH (T-RO1-DK090989, 1UL1-RR029893, UL1-TR000038), the Diane Belfer Program in Human Microbial Ecology, the Philip and Janice Levin Foundation, the Michael Saperstein Fellowship, and institutional funds provided by the J. Craig Venter Institute, and the NYU Genome Technology Center. We thank N. Javitt for advice and J. Chung for technical assistance.

Author Contributions I.C. and M.J.B. designed the study; I.C., L.C., S.Y., Z.G., D.M., I.T. and K.R. performed experiments; B.A.M. and K.L. performed sequencing and sequencing analysis; J.Z. performed microarray analyses; I.C. and H.L. performed statistical interpretation and analyses; A.V.A. performed bioinformatics analyses and interpretation; I.C. and M.J.B. took primary responsibility for writing the manuscript.

Author Information Reprints and permissions information is available at www.nature.com/reprints. The authors declare no competing financial interests. Readers are welcome to comment on the online version of the paper. Correspondence and requests for materials should be addressed to M.J.B. (martin.blaser@med.nyu.edu).

METHODS

Mouse husbandry. Female C57BL/6J mice were obtained at weaning (21 days of life) from Jackson Laboratories and allowed to adjust to the NYU animal facility for 1 week. Mice were weighed at the beginning of each experiment and distributed five per cage so that mean weights in each cage were equal. In each experiment, each study group (control or antibiotic(s)) was composed of ten mice. The mice were allowed ad libitum access to food and water and were maintained on a 12-h light/dark cycle and fed standard laboratory chow (Purina Mills International Diet no. 5001). The protocol was approved by the New York University School of Medicine Institutional Animal Care and Use Committee (IACUC).

Antibiotic dosing. Beginning on day 28 of life, mice were given standard water (pH 6.8) or water containing one of the following antibiotic regimens: penicillin VK, vancomycin, penicillin VK plus vancomycin, and chlortetracycline. Doses were adapted from the FDA Green Book and generally were in the mid-range of those approved for use in agriculture[6,7,37]. To simplify administration, the antibiotics were added to drinking water at a dose of 1 μg antibiotic per g body weight of the mice in the cage, based on the calculation that daily water intake is proportional to body weight. In previous studies, the daily water intake in C57BL/6J mice averaged 15 ml water per 100 g body weight[44]. Water containers were changed twice weekly to supply fresh antibiotics.

Mouse measurements and phenotypes. Three times a week, each mouse was weighed twice on an electronic scale tared between all measurements. The quantity of feed consumed per cage was measured and average daily feed intake calculated. Feed efficiency was calculated by dividing mean weight gain by mean daily feed consumed per mouse. Faecal pellets were collected every week and stored at −20 °C until processing. Body composition was determined using dual energy X-ray absorptiometry (DEXA) with a Lunar PIXImus II mouse densitometer (GE Medical Systems) at weeks 3 and 7. Each mouse was scanned individually and data collected on fat composition, lean body mass, per cent body fat, and bone mineral density. MRI experiments were performed on a 7 tesla MRI system gated on respiratory rate. During the scan, anaesthesia was maintained with 1.5% isoflurane in oxygen. The animal body temperature was maintained at 37 °C (±1 °C) during the scan by directing a thermostatically controlled warm air source. Images captured were separated into fat and lean tissue using the IDEAL Dixon method based on chemical shift properties[45] and total body fat percentage (volume/volume) was calculated by merging fat and lean images in MRIcron software (http://www.mccauslandcenter.sc.edu/mricro/mricron/). Weight values were validated by comparisons with scale weight and fat% values with MRI-determined fat% (Supplementary Fig. 1). Mice were killed by CO_2 inhalation and cervical dislocation and blood was collected via cardiac puncture. The blood was separated into serum and whole cells. Necropsy was performed on each mouse and caecal contents, liver, serum and visceral adipose tissue were collected. All samples were snap-frozen and stored at −80 °C until processing.

Statistical comparison of growth rates. From the experiment shown in Supplementary Fig. 4, the plots of group means of total, fat and lean mass over time were fitted with the following linear spline model with a common knot at week 26:

$$E(Y) = \beta_0 + \beta_1 \text{group} + \beta_2 \text{week} + \beta_3 (\text{week} - 26)_+ + \beta_4 \text{group} \times \text{week} + \beta_5 \text{group} \times (\text{week} - 26)_+$$

where group = 0 indicates the control group and group = 1 indicates the STAT group, and $(x)_+$ is defined as a function that equals x when x is positive and is equal to zero otherwise. With this model we performed the group comparisons at baseline, before week 26 and to examine patterns of change over time through tests H_0: $\beta_1 = 0$, H_0: $\beta_4 = 0$ and H_0: $\beta_4 = \beta_5 = 0$, respectively. The MIXED procedures of SAS software (version 9.2; SAS Institute, Inc.) were used to perform the tests and calculate the estimates.

Hormone measurements. Blood cells and serum were separated through centrifugation (3,000*g* for 10 min at 4 °C) and the serum frozen at −70 °C. Serum specimens (100 μl) were examined using the Millipore Mouse Gut Hormone Panel (Millipore Corp.) using a Luminex 200 (Millipore) analyser. The panel was custom-designed to assess for glucose-dependent insulinotropic peptide (GIP), insulin, IGF-1, peptide YY, ghrelin and leptin.

Glucose tolerance test. Control and STAT mice were fasted for 12 h during study week 6 (week 10 of life) and weights determined by electronic scale. Blood glucose at baseline was measured using an Accu-Chek Compact Plus glucometer (Roche). The mice then were challenged with 2 mg glucose per g body weight, given intraperitoneally, as previously described[46], and blood glucose levels determined 30, 60 and 120 min later. Area under curve (AUC) calculations were used to compare the STAT and control groups between 30 and 60 min.

DNA extraction. DNA extractions from caecal contents and faecal pellets were performed using the Qiagen QIAmp DNA stool extraction kit (Qiagen) per the manufacturer's protocol. Total extracted DNA was quantified using a Nanodrop 1000 (Thermo Scientific). PCR to confirm bacterial DNA extractions was performed using the 8F/1510R bacterial primers for 16S rRNA[47,48].

Quantitative PCR amplification. After genomic DNA extraction and quantification, samples were prepared for amplification and sequencing at the JCVI Joint Technology Center (JTC). Genomic DNA sample concentrations were normalized to ~5–10 ng μl^{-1}. The v3 region of the 16S rRNA gene was amplified using forward primer 341F (5′-CCTACGGGAGGCAGCAG-3′) and reverse primer 534R (5′-ATTACCGCGGCTGCTGG-3′) to which a 'CG' on the 5′ end of the primer followed by symmetrical 10-nucleotide barcodes were included as part of the primer design (5′- CGN(10)+16S primer-3′). Barcoded primer designs were completed using a set of algorithms developed at the JCVI. This design allowed for the inclusion of a unique barcode to each sample at the time of PCR so that the tagged samples could be multiplexed for sequencing. A total of 96 barcodes were used. Every effort was made to prevent contamination of PCR reactions with exogenous DNA including a set of reactions in a laminar flow hood. PCR reactions were completed as follows (per reaction): 1 μl of gDNA, 1× final concentration of Accuprime PCR Buffer II (Invitrogen), 250 mM betaine, 200 nM forward and reverse primers, 0.5 units of Accuprime Taq DNA Polymerase High Fidelity (Invitrogen), and nuclease-free water to bring the final volume to 10 μl. PCR cycling conditions were: initial denaturation of 2 min at 95 °C followed by 25 cycles of 10 s at 95 °C, 20 s at 63 °C and 30 s at 72 °C. A negative control (water blank) reaction also was included and examined after 30 cycles. PCR reactions were visualized on 1% agarose gels and quantified using a Tecan SpectraFluor Plus (Tecan Group Ltd) before normalization and pooling of samples for sequencing.

454-FLX read quality filtering. After the completion of sequencing, a read processing pipeline involving a set of modular scripts designed at the JCVI was used for deconvolution, trimming and quality filtering[49]. First reads were deconvoluted, or assigned to samples, based on their unique 10-nucleotide barcode, allowing ≤1-nucleotide mismatch to the reference barcode sequence and ≤6 primer sequence mismatches, using the EMBOSS program fuzznuc to locate barcodes and primer sequences on each read. To eliminate spurious hits, the distance between detected barcode and primer were required to be ≤3 nucleotides. Barcodes then were trimmed from the sequence and remaining sequences which failed to have barcodes detected then were filtered. After deconvolution, primer sequences detected at >75% identity were trimmed and those without valid primers detected were eliminated. Reads with an average length of <100 nucleotides or with any Ns were removed. A BLASTN quality check[50] was performed against a small internal data set of 200 16S reads to remove sample reads substantially inconsistent with 16S gene sequences. The criteria were that >30% of the query must be covered by the alignment with a minimum of 60 nucleotides of identity. Passing reads were subsequently examined using a modified version of the RDP Chimera Check in which candidate chimaeras were identified based only on reads that were sequenced within the sample. Final sequence data have been deposited in the NIH Sequence Read Archive (http://www.ncbi.nlm.nih.gov/sra). Accession numbers for all primary sequencing data are available from the NCBI under BioProject 168618.

Sequence analyses. The pooled sample was cleaned using the Agencourt AMPure system (Beckman Coulter Genomics). The A and B adapters necessary for sequencing with 454-FLX Titanium chemistry (Roche) were subsequently ligated to the sample pool after PCR following standard manufacturer protocols. Library construction, emPCR, enrichment, and 454 sequencing were performed by following the vendor's standard operating procedures with some modifications. Specifically, quantitative PCR was used to accurately estimate the number of molecules needed for emPCR. We also used automation (BioMek FX) to 'break' the emulsions after emPCR and we used butanol to enable easier sample handling during the breaking process.

Statistical and computational sequence analysis. Quality-filtered sequences (see Supplementary Methods) were pre-processed through the QIIME pipeline[51] involving: (1) clustering the sequences into operational taxonomical units (OTUs) using the UCLUST program[52] at a 97% similarity threshold; (2) taxonomically assigning each OTU by selecting a representative sequence from each OTU-cluster and running RDP Classifier[53] with 80% bootstrap confidence; (3) aligning representative sequences for each OTU with the Greengenes core-set alignment template using PyNAST[54]; (4) building a phylogenetic tree for the OTUs using the FASTTREE program[55]; and (5) calculating weighted Unifrac beta-diversity indices[56]. We extracted the OTU absolute abundance table and weighted Unifrac beta-diversity matrix[56,57] from the pipeline for further analysis in the R statistical programming environment[58,59]. The rarefactions for diversity indices and species richness were calculated in the R statistical programming environment[59,60] using Community Ecology Package Vegan. The OTU absolute abundances were converted to relative abundances by normalizing to total

sequence count per sample analysed. The resulting relative abundance matrix was used to produce heat maps and major taxa bar plots. (Code available on the NYU Center for Health Informatics and Bioinformatics website http://www.nyuinformatics.org/research/labs/microbiomics.) All data are presented as mean ± s.e.m., unless otherwise indicated for groups without normal data distribution (median ± IQR). Comparisons of medians between non-normally distributed groups were performed using the Mann–Whitney *U*-test or Kruskal–Wallis analysis of variance test for simultaneous comparisons of more than two groups. Multivariate analysis of taxonomic distributions among groups was performed using double-principal coordinate analysis (DPCoA), as described[61,62]. To compare the inter- and intragroup statistical differences in beta diversity, we used a two-sided *t*-test. We ensured that possible violations of *t*-test assumptions when comparing beta-diversity did not affect statistical decisions (Supplementary Tables 4 and 5). *P* values <0.05 were considered to be significant.

Comparison of intra- and intergroup weighted Unifrac distances. Statistical comparison of intra- and intergroup weighted Unifrac distances requires application of a statistical test appropriate for the data. In our analysis, we apply a series univariate two-sample *t*-tests corrected for multiple comparisons for this purpose. However, application of the *t*-test requires that certain assumptions are satisfied, of which normality is the most notable. We inspected normal quantile plots to determine the extent of the linear trend, which provides evidence for the similarity of the empirical distribution to normal. We formally supplement this visual diagnostic with normality testing. Normality testing for the purpose of satisfying test assumptions is difficult in statistical analyses because normality can only be rejected and never confirmed; thus, it usually is not done in typical analyses of this sort. However, we performed the Shapiro–Wilk's test for normality on inter- and intragroup weighted UniFrac distances. Although in many cases normality could be rejected depending on the desired alpha level (Supplementary Table 4), we were able to identify long regions of linearity in each case to establish that the peak of the distributions is approximately normally distributed. For final assurance that decisions based on *t*-test are not affected by possible violations of the normality assumption, we also performed Mann–Whitney tests which (after adjustment for multiple comparison adjustment) provided the same rejections of the null hypothesis as for the original *t*-tests (Supplementary Table 5).

Quantitative PCR. Quantitative PCR assays to assess for taxa of interest were performed on a Rotor Gene 3000 quantitative PCR cycler using the LightCycler FastStart DNA Master PLUS SYBR Green I kit (Roche) according to the manufacturer's instructions. Quantitative assays to assess total microbial census were performed for Bacteria using 16S rRNA and Fungi using ITS sequences. Quantitative assays were also performed for butyryl CoA transferase (BCoAT) and formyltetrahydrofolate synthetase (FTHFS), using degenerate primers. All primer sequences are provided in Supplementary Table 1. Values were normalized based on total Bacteria 16S copies.

Hepatic triglyceride measurements. For triglyceride measurements, hepatic tissue was homogenized at 4 °C in RIPA lysis buffer (Sigma-Aldrich) and lipids extracted using a chloroform/methanol (2:1) method, evaporated, and dissolved in 2-propanol[63]. Triglyceride concentration was assayed using the enzymatic hydrolysis of triglycerides by lipase to glycerol and free fatty acids and quantification by colorimetric assay (Sigma-Aldrich).

Hepatic gene expression profiling and data analysis. Total DNA and total RNA was extracted from the mouse liver by the Wizard Genomic DNA purification Kit (Promega) and RNeasy Mini Kit (Qiagen), respectively, according to the manufacturer's instructions. Total RNA was reverse transcribed to cDNA using the Verso cDNA Synthesis Kit (Thermo Scientific). To generate standards for each target gene expression analysis, the DNA or cDNA region of interest was PCR-amplified and the PCR product was cloned using the pGEM-Teasy vector system (Promega). qPCR was performed with a LightCycler 480 SYBR Green I Master (Roche) and run in a LightCycler 480 system (Roche). Target mRNA was normalized to GAPDH mRNA as an internal control in each sample.

Expression profiling of the STAT and control animal groups ($n = 6$ each) was performed using the Affymetrix Genechip system (Affymetrix). Total RNA quality and quantity were determined using the Agilent 2100 Bioanalyser and Nanodrop ND-1000. Total RNA (100 ng) was used to prepare cDNA following the Affymetrix 3′IVT Express Kit labelling protocol (Affymetrix). Standardized array processing procedures recommended by Affymetrix were performed, including hybridization, fluidics processing and scanning of the Affymetrix MG-430 2.0 arrays. GeneSpring GX11 software (Agilent Technologies) was used to normalize the raw data (Affymetrix CEL files) by Robust Multichip Average algorithm (RMA). Gene set enrichment analysis (GSEA)[43] was used to identify significantly enriched gene expression patterns underlying fatty acid and lipid metabolism, by querying the C2 (curated pathways) and C5 (Gene Ontologies) categories of the GSEA MolSig v.3 database. The microarray data have been submitted in the MIAME-compliant format to the NCBI GEO public database (http://www.ncbi.nlm.nih.gov/geo/) under the identifier GSE38880.

Histology and immunohistochemistry. Fat tissues of mice were collected and frozen at −80 °C before being thawed and embedded in optimum cutting temperature (OCT) medium. Sections were cut in 5 μm thickness for staining with haematoxylin and eosin. Immunohistochemistry was performed on frozen formalin-fixed tissues using rat anti-mouse CD68 (AbDSerotec). In brief, sections were thawed at room temperature for 30 min, fixed in 10% NBF for 15 min, rinsed in distilled water, and soaked in reaction buffer for 15 min. Antibody incubation and detection were carried out at 37 °C on a NeXes instrument (Ventana Medical Systems) using Ventana's reagent buffer, endogenous biotin blocking kit and detection kits unless otherwise noted. Endogenous peroxidase activity was blocked with hydrogen peroxide. Antibodies against CD68 were diluted 1:75 and were incubated for 30 min. CD68 was detected using a biotinylated rabbit anti-rat antibody (Vector Laboratories) diluted 1:4,000 and incubated for 30 min. After secondary antibody application, streptavidin-horseradish-peroxidase conjugate was applied. The complex was visualized with 3,3-diaminobenzidene and enhanced with copper sulphate. Slides were washed in distilled water, counterstained with haematoxylin, dehydrated and mounted with permanent media. Appropriate positive and negative controls were included with the sections studied.

Histological and immunohistochemical analyses. Histology and immunohistochemistry slides were digitally scanned at ×40. From each section (STAT, $n = 10$; control, $n = 10$), 10 high-power fields (HPF) were selected by a single observer. Copies of each of the images were provided to two independent individuals blind to the experimental design who counted adipocytes or $CD68^+$ macrophages in each HPF using ImageJ (http://rsbweb.nih.gov/ij/). The counts were compared between the two investigators and the mean number of adipocytes or $CD68^+$ macrophages per HPF for control and STAT mice were compared using the Student's *t*-test.

Gas chromatographic analysis. Mouse faecal pellets were collected at week 6 of the experiment and frozen until analysed. Single pellets were weighed and homogenized in 100 μl of deionized water for 3 min. The pH of the suspension was adjusted to 2–3 by adding 5 M HCl at room temperature for 10 min with intermittent shaking. The suspension was transferred into a polypropylene tube and centrifuged for 20 min at 3,000g, yielding a clear supernatant. The internal standard, 2-ethylbutyric acid (TEBA), was added into the supernatant at a final concentration of 1 mM. Chromatographic analysis used the Shimadzu QP-500 GC/MS system (Shimadzu). A fused-silica capillary column (30m, 0.52mm, 0.50μm) with a free fatty acid phase (DB-FFAP 125-3237, J&W Scientific, Agilent Technologies Inc.) was used for analysis. Helium was the carrier at a flow rate of 14.4 ml min^{-1}. The initial oven temperature (100 °C) was maintained for 30 s, raised to 180 °C at 8 °C min^{-1} and held for 60 s, then increased to 200 °C at 20 °C min^{-1} and held for 5 min. The flame ionization detector and injection port were kept at 240 and 200 °C, respectively. The flow rates of hydrogen, air, and nitrogen were 30, 300 and 20 ml min^{-1}, respectively. The injected sample volume for GC analysis was 1 μl, and each analysis had a run time of 32 min[64].

Metabolic cage measurements. C57BL/6J mice were singly housed in Techniplast Type 304 metabolic cages (Techniplast). Mice had unrestricted access to 45% HFD powdered chow and STAT or control water, as appropriate. There was a 2-day acclimatization period, followed by 3 days of measurements. Measurements recorded were body weight, food and water consumed, and faeces and urine produced. Total faeces and urine were collected for analysis. Calories consumed were calculated by weight of food consumed and 4,057 cal g^{-1} as per the manufacturer's instructions (Research Diets). Calories excreted were calculated based on total faeces produced and calorimetric analysis of a homogenate pellet incorporating all faeces produced per mouse from each 24-h period.

Bomb calorimetry. Calorimetric measurements were obtained using a Parr 6725 Semi-micro calorimeter. Faecal pellets obtained during week 6 of the experiment were dehydrated overnight at 56 °C with a silica gel desiccant. All pellets studied had minimum dry weights >12 mg. The calorimeter was calibrated using multiple benzoic acid standards intermixed with the experimental measurements in each day's run. Corrections were made for sulphur content and fuse length; final results were expressed as calories per gram dry weight.

44. Harkness, J. E. & Wagner, J. E. *The Biology and Medicine of Rabbits and Rodents* 3rd edn (Lea and Febiger, 1989).
45. Reeder, S. B. *et al.* Iterative decomposition of water and fat with echo asymmetry and least-squares estimation (IDEAL): application with fast spin-echo imaging. *Magn. Reson. Med.* **54,** 636–644 (2005).
46. Andrikopoulos, S., Blair, A. R., Deluca, N., Fam, B. C. & Proietto, J. Evaluating the glucose tolerance test in mice. *Am. J. Physiol. Endocrinol. Metab.* **295,** E1323–E1332 (2008).
47. Favier, C. F., Vaughan, E. E., De Vos, W. M. & Akkermans, A. D. L. Molecular monitoring of succession of bacterial communities in human neonates. *Appl. Environ. Microbiol.* **68,** 219–226 (2002).

48. Martínez-Murcia, A. J., Acinas, S. G. & Rodriguez-Valera, F. Evaluation of prokaryotic diversity by restrictase digestion of 16S rDNA directly amplified from hypersaline environments. *FEMS Microbiol. Ecol.* **17,** 247–255 (1995).
49. Li, K. *et al.* ANDES: Statistical tools for the ANalyses of DEep Sequencing. *BMC Res. Notes* **3,** 199 (2010).
50. Altschul, S. F., Gish, W., Miller, W., Myers, E. W. & Lipman, D. J. Basic local alignment search tool. *J. Mol. Biol.* **215,** 403–410 (1990).
51. Caporaso, J. G. *et al.* QIIME allows analysis of high-throughput community sequencing data. *Nature Methods* **7,** 335–336 (2010).
52. Edgar, R. C. Search and clustering orders of magnitude faster than BLAST. *Bioinformatics* **26,** 2460–2461 (2010).
53. Wang, Q., Garrity, G. M., Tiedje, J. M. & Cole, J. R. Naive Bayesian classifier for rapid assignment of rRNA sequences into the new bacterial taxonomy. *Appl. Environ. Microbiol.* **73,** 5261–5267 (2007).
54. Caporaso, J. G. *et al.* PyNAST: a flexible tool for aligning sequences to a template alignment. *Bioinformatics* **26,** 266–267 (2010).
55. Price, M. N., Dehal, P. S. & Arkin, A. P. FastTree 2–approximately maximum-likelihood trees for large alignments. *PLoS ONE* **5,** e9490 (2010).
56. Lozupone, C., Lladser, M. E., Knights, D., Stombaugh, J. & Knight, R. UniFrac: an effective distance metric for microbial community comparison. *ISME J.* **5,** 169–172 (2010).
57. Lozupone, C. & Knight, R. UniFrac: a new phylogenetic method for comparing microbial communities. *Appl. Environ. Microbiol.* **71,** 8228–8235 (2005).
58. Gentleman, R. C. *et al.* Bioconductor: open software development for computational biology and bioinformatics. *Genome Biol.* **5,** R80 (2004).
59. Ihaka, R. & Gentleman, R. R: a language for data analysis and graphics. *J. Comp. Graph.* **5,** 299–314 (1996).
60. Gentleman, R. C. *et al.* Bioconductor: open software development for computational biology and bioinformatics. *Genome Biol.* **5,** R80 (2004).
61. Pavoine, S. & Bailly, X. New analysis for consistency among markers in the study of genetic diversity: development and application to the description of bacterial diversity. *BMC Evol. Biol.* **7,** 156 (2007).
62. Pavoine, S., Dufour, A. B. & Chessel, D. From dissimilarities among species to dissimilarities among communities: a double principal coordinate analysis. *J. Theor. Biol.* **228,** 523–537 (2004).
63. Hong, F. *et al.* Interleukin 6 alleviates hepatic steatosis and ischemia/reperfusion injury in mice with fatty liver disease. *Hepatology* **40,** 933–941 (2004).
64. Zhao, G., Nyman, M. & Jonsson, J. A. Rapid determination of short-chain fatty acids in colonic contents and faeces of humans and rats by acidified water-extraction and direct-injection gas chromatography. *Biomed. Chromatogr.* **20,** 674–682 (2006).